DTU Library

Stability Oriented Design of Model Predictive Control for DC/DC Boost Converter

Li, Yuan; Sahoo, Subham; Dragicevic, Tomislav; Zhang, Yichao; Blaabjerg, Frede

Published in:
IEEE Transactions on Industrial Electronics

Link to article, DOI:
10.1109/TIE.2023.3247785

Publication date:
2024

Document Version
Peer reviewed version

Citation (APA):
Li, Y., Sahoo, S., Dragicevic, T., Zhang, Y., & Blaabjerg, F. (2024). Stability Oriented Design of Model Predictive Control for DC/DC Boost Converter. *IEEE Transactions on Industrial Electronics*, *71*(1), 922-932. https://doi.org/10.1109/TIE.2023.3247785

This article has been accepted for publication in IEEE Transactions on Industrial Electronics. This is the author's version which has not been fully edited and content may change prior to final publication. Citation information: DOI 10.1109/TIE.2023.3247785

Stability Oriented Design of Model Predictive Control for DC/DC Boost Converter

Yuan Li, *Student Member, IEEE,* Subham Sahoo, *Member, IEEE,* Tomislav Dragičević, *Senior Member, IEEE,* Yichao Zhang, *Student Member, IEEE,* and Frede Blaabjerg, *Fellow, IEEE*

***Abstract*—Model predictive control (MPC) based on long prediction horizons can address the inherent non-minimum phase (NMP) behavior issue of DC/DC boost converters. However, the response time of the controller will increase since the long prediction horizons result in a high computational burden. To solve this problem, a non-minimum phase behavior improving (NPI) MPC with a single prediction horizon is proposed in this paper. Firstly, the actual cause behind the NMP behavior is analyzed. Afterward, the difference equation is modified according to the analysis and then used in the NPI-MPC. In addition, a fixed switching frequency is generated based on the value of the duty cycle, which is realized in the NPI-MPC algorithm and a modulation. Moreover, a weighting factors-design guideline based on the stability criterion of a Jacobian matrix is provided. It effectively reflects the impact and sensitivity of different weighting factors on stability. Finally, we conclude this paper by validating the proposed NPI-MPC method and the weighting factors-design guidelines with the results obtained under experimental conditions.**

***Index Terms*—Model predictive control; non-minimum phase behavior; boost converter; fixed switching frequency; weighting factors.**

I. Introduction

WITH the increased renewable energy generation, especially photovoltaics (PV), and energy storage modules, DC microgrids are gaining more attention [1]-[4]. Since DC/DC boost converters can provide a higher output voltage to be integrated into a standardized system, they act as one of the most common interfaces in DC microgrids [5].

Because the inherent non-minimum phase (NMP) behavior in the boost converter, it poses challenges in the design of the controller. Compared with the traditional PI controller [6]-[7], non-linear controllers can describe the nonlinear nature of the converters and exhibit better dynamic performance [8]-[10]. Among these control methods, the conventional sliding-mode control utilizes the inductor current control scheme for the boost converter, which performs good robustness. However, it will make the control signal calculation complex and suffer from the chattering issue [8]-[9]. Considering fuzzy controllers, they show better nonlinear representation ability and cope well with the NMP issue. However, the number of fuzzy rules is designed empirically which can not apply to different conditions [10]. Moreover, if the fuzzy rules increase, the control performance is better but with a heavy computational burden. Recently, the model predictive control (MPC) has extended its applications in power converters with fast response, explicit control constraints, and easy implementation, which attracts more attention [11]-[13].

To address the NMP problem in a boost converter, previous studies prefer to utilize long prediction horizons based MPC [14]-[16], resulting in high computational complexity and long control response time. To arrange for a short computation time, it can be carried out from the decoding aspect and the control aspect. For the decoding aspect, the sphere decoding algorithm is incorporated into the MPC [17]-[19], which avoids traversing all candidates. However, the digital controller needs to be designed to realize the decoding algorithm [19]. From the control aspect, the direct solution is to adopt the single prediction horizon [20]-[22]. An input state linearization is used to solve the NMP behavior for the boost converter [20]. In addition, only inductor current controlled based MPC with a single prediction horizon is presented to weaken the influence of NMP behavior [21]. However, an observer should be adopted to compensate for the dynamic performance's degradation resulting from the lack of capture for the output voltage varying. A PI generated current reference based MPC is proposed to perform an accurate control [22]. Nevertheless, the dynamic response speed will deteriorate with the introduction of the PI module. Therefore, an efficient and simply designed MPC is urgent.

Another problem in conventional MPC is the inherent variable switching frequency. When the switching frequency varies during the operation, it will lead to non-uniform inductor current ripples and may lead to a saturation boundary which complicates the design of inductance and in general increases the maximum ripple in the inductor current. Besides, when the frequency changes, the converter may change from the current continuous conduct mode to the discontinuous conduct mode, which brings challenges to the predictive model of MPC [21], [22]. Hence, to generate a fixed switching frequency, the modulation is commonly used in MPC which is regarded as the continuous control set (CCS)-MPC [21]. The switching frequency is decided by the frequency of the carrier wave. Another modulation free MPC is provided for the DC/DC SEPIC converter [22]. By introducing the inductor current variation into the cost function, it achieves control of the fixed switching frequency. However, the switching frequency will fluctuate during the variation of the system's parameters.

Although the MPC algorithm is widely used for power converters, weighting factors design issues that are closely related to its performance have not been fully addressed [23]. Hence, some methods for coping with the weighting factors design issues are produced [24]-[27]. For instance, to avoid utilizing the weighting factors, the cost function is designed as the error between the single predicted value and

This article has been accepted for publication in IEEE Transactions on Industrial Electronics. This is the author's version which has not been fully edited and content may change prior to final publication. Citation information: DOI 10.1109/TIE.2023.3247785

its reference [24]. Nevertheless, it cannot be realized with multi-objective optimization issues. Another approach utilizes a fuzzy multi-criteria decision making method controlling the direct matrix converter [25]. Instead of the weighting factors, the membership functions are adopted, which are defined as the relationship between the predicted value, and the maximum, and minimum values of the state variables. Finally, the optimal control switching state is decided by the value of the membership function with all candidates. However, it still needs priority coefficients for control objectives to be chosen.

Normally, the selection of weighting factors are empirical, which lacks of design guidelines. With the mature of the artificial intelligence (AI) techniques, another solution gets more attentions. The AI-based solution is with numerous simulations and concluds with an optimal combination of weighting factors [12], [27]. Ref [27] utilizes an ANN-based algorithm to select the weighting factors, which costs less time than the numerous simulations-based method. In summary, the existing weighting factors design methods are mostly dependent on large numbers of data, where the design process is based on a data-driven model instead of a system model. Thus, it is necessary to find a design framework, which can reveal the essence of the effects of the weighting factors.

To address the above mentioned challenges, this paper proposes a non-minimum phase behavior improving (NPI)-MPC algorithm for a boost converter with a single prediction horizon. The main contributions are listed as:

1) A modified difference equation for the inductor current is proposed after analyzing the actual cause behind the NMP behavior. Based on this, an NPI-MPC with a single prediction horizon is proposed, where the NMP behavior has substantially less influence in the system. Moreover, this paper derives the optimal duty cycle from the proposed MPC and then generates a fixed switching frequency, which acts as a fundamental requirement for further modeling and stability analysis.

2) The model of the NPI-MPC controlled boost converter is presented. Based on the model, this paper proposes a weighing factor selection method which utilizes a Jacobian matrix to assess the stability. Finally, by calculating the eigenvalues of the Jacobian matrix, the selection of the weighting factors and the design of the parameters are provided to guarantee stability.

The rest of the paper is organized as follows. Section II illustrates the discrete model of the boost converter. Section III proposes the NPI-MPC algorithm. Section IV presents the model of the proposed method and gives the guideline for selecting weighting factors. Experiments are supplemented in Section V. Section VI concludes the paper.

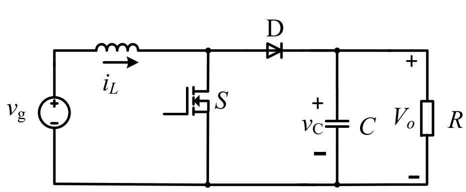

Fig. 1. DC-DC boost converter.

II. DC-DC Boost Converter Description

The studied system is shown in Fig. 1. The equivalent diagram of the boost converter in different switching periods is demonstrated in Fig. 2. According to the operating principle, the following equation can be obtained:

$$\frac{dV_o}{dt} = \frac{1-d}{C} i_L(k) - \frac{1}{RC} V_o(k) \tag{1}$$

$$\frac{di_L}{dt} = \frac{1}{L} V_g - \frac{1-d}{L} V_o(k) \tag{2}$$

where d is the duty cycle. Assuming that the sampling frequency is relatively high, the state variables dVo/dt in (1) can be transformed into a discrete-time equation with the classical forward Euler approximation method. It is expressed as:

$$V_o(k+1) = V_o(k) + \frac{1-d}{C} i_L(k) T_s - \frac{1}{RC} V_o(k) T_s \tag{3}$$

Similarly, the difference equation of the inductor current can be derived as:

$$i_L(k+1) = i_L(k) - \frac{1-d}{L} V_o(k) T_s + \frac{1}{L} V_g T_s \tag{4}$$

Based on (3) and eq. (4), the output voltage and inductor current in the next sampling time can be predicted which also provide the control objectives of MPC.

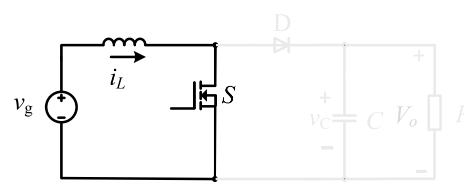

(a) 0-dT_s.

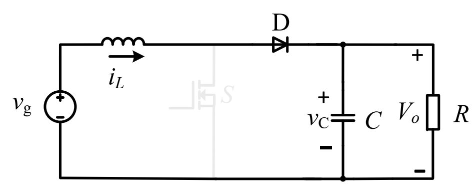

(b) dT_s-T_s.

Fig. 2. Equivalent diagram of boost converter during different periods.

III. Proposed NPI-MPC Algorithm

This section explains the design process of the proposed NPI-MPC algorithm in the following steps. Firstly, the NMP behavior with direct voltage/current MPC is presented and the actual cause of this instability is analyzed. Based on the analysis, the proposed NPI-MPC is implemented.

A. Analysis of Direct Voltage/Current MPC

Usually, the control purpose of the converter is to provide a stable and tightly regulated output voltage for the load. Thus, the most direct cost function is to control the output voltage. Then, we can obtain:

$$J = \sum_{i=1}^{N} (V_o(k+i) - V_o^*)^2 \tag{5}$$

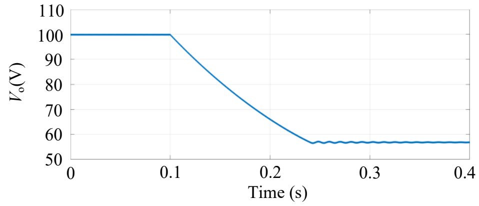

Fig. 3. Output voltage fails to track the reference at 0.1 s in the boost converter with a single prediction horizon.

where N is the prediction horizon. However, as Fig. 3 shows, when the MPC algorithm adopts a single prediction horizon (from N=3 to N=1) at 0.1 s, the output voltage falls and fails to track the voltage reference which is 100 V, and finally stays at 57 V. Although the long prediction based MPC can improve this instability, the computation burden will further increase. Fig. 4 shows the stages with different prediction horizons based on MPC. As seen, with the increase of the prediction horizon, the cost function contains more predicted values, which are obtained by the prediction model in a stepwise manner. Hence, it is obvious that the computation process with a single prediction horizon is with less time consumption and computation burden as compared to long prediction horizons. Another approach used widely is the direct inductor current MPC, which is based on the following prediction model [21]-[22]:

$$J = (i_L(k+i) - i_L^*)^2 \tag{6}$$

However, without compensating the inductor current reference, a stationary error still exists as Case II in Fig.5 shows. Therefore, the MPC algorithm based on the above cost functions cannot regulate a preset output voltage.

B. Analysis of the Non-minimum Phase Dynamics

To address the above problem without consuming a long prediction horizon, the reason behind the NMP behavior should be studied first. The following equation shows the relationship between the duty cycle and the output voltage transfer function of the boost converter in the s-domain [10]:

$$G_{vd}(s) = \frac{V_g}{1-D_1}\frac{(1-D_1)^2R - Ls}{[LCRs^2 + Ls + 1 - D_1)^2R]} \tag{7}$$

Here, D_1 is the stable state value of the duty cycle, and s represents the s-domain variable. Since the zero in (7) which equals $(1-D_1)^2R/L$ lies in the right half-plane, the boost converter is an NMP system. Due to the conventional unconstrained one short horizon, MPC behaves as an input-output linearizing controller [28]. When using the single prediction horizon cost function in (5), it will lead to instability because of the unstable zero dynamics that exists in the NMP system [20].

Although the NMP behavior exists in (7), when we consider the relationship between the duty cycle and the inductor current transfer function of a boost converter in the s-domain, we obtain:

$$G_{id}(s) = \frac{V_g}{1-D_1}\frac{CRs + 2}{[LCRs^2 + Ls + R(1-D_1)^2]} \tag{8}$$

As evident from (8), the zero is in the left half-plane, which means if only the inductor current is introduced in the control loop to generate the control signal, the system is stable. It seems that the output voltage is not necessary for this cost function and the NMP behavior can be avoided. However, when considering the difference equation in (4), it is intuitive that the output voltage is also adopted to generate the duty cycle. Hence, without modifying the prediction differential equation, the NMP behavior will still severely influence the system.

C. Design of the Proposed NPI-MPC

Usually, in the conventional PI control method, through the design of the compensation network and parameters whose essence is to cancel the pole-zero placement in the right-half plane, the influence of the unstable behavior will be reduced. Inspired by this, the design of the prediction differential equation can also be realized to weaken the influence of NMP behavior. Besides, the dynamic response across the converter output should not be sacrificed. To this end, this paper proposes a difference equation for the inductor current. According to the power balance, the total input power equals the output power neglecting the power conversion losses, we obtain:

$$V_g i_L(k) = V_o(k) i_o(k) \tag{9}$$

where $i_o(k)$ is the output current in the real system. And the difference equation can be transformed as:

$$\begin{cases} i_L(k+1) = i_L(k) - (\frac{1-d}{L}\sqrt{i_L(k)V_g\frac{V_o(k)}{i_o(k)}} + \frac{1}{L}V_g)T_s \\ V_o(k+1) = V_o(k) + (\frac{1-d}{C}i_L(k) - \frac{i_o(k)}{C})T_s \end{cases} \tag{10}$$

As seen, (10) avoids only using the output voltage $V_o(k)$ at k instant when predicting the inductor current $i_L(k+1)$ in the next sampling time. The item $V_o(k)/i_o(k)$ in (10) equals the load resistance and it will not introduce instability into the system. Besides, to avoid the sluggish dynamic performance when the output voltage reference or load is changed, the output voltage $V_o(k+1)$ is also predicted. Hence, based on the proposed prediction model, it can not only weaken the NMP behavior accompanying the boost converter but can also ensure the dynamic performance of the system.

The cost function is established based on the predicted values and the desired reference. Thus, the cost function J contains the predicted value from (10) and uses the quadratic error as:

$$\begin{aligned} J =& (i_L(k) - \frac{1-d}{L}\sqrt{i_L(k)V_g\frac{V_o(k)}{i_o(k)}}T_s + \frac{1}{L}V_gT_s - i_L^*)^2 \\ &+ (V_o(k) + \frac{1-d}{C}i_L(k)T_s - \frac{i_o(k)}{C}T_s - V_o^*)^2 \end{aligned} \tag{11}$$

where, the output voltage reference V_o^* is predefined and the inductor current reference i_L^* is determined as $V_o^* i_o/V_g$. As seen, the studied system contains two control objectives. To compensate for the difference in the natural characteristics of different control objectives and ensure control performance,

This article has been accepted for publication in IEEE Transactions on Industrial Electronics. This is the author's version which has not been fully edited and content may change prior to final publication. Citation information: DOI 10.1109/TIE.2023.3247785

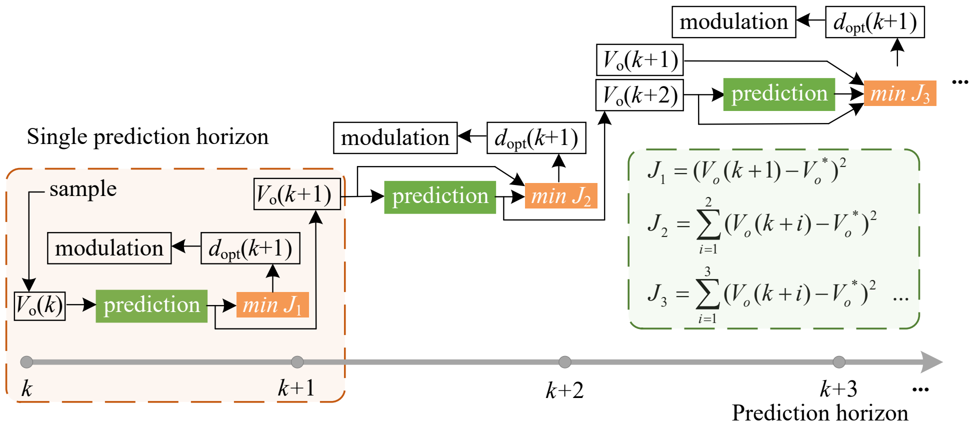

Fig. 4. Computation process with different prediction horizons.

TABLE I
SYSTEM PARAMETERS.

Parameters	Symbols	Values
Input voltage	V_g	50 V
Output voltage	V_o	100 V
Inductance	L	1 mH
Capacitor	C	2000 μF
Switching cycle	T_s	50 μs
Output power	P	200 W
Reference inductor current	i_L^*	$V_o^* i_o(k)/V_g$
Reference output voltage	V_o^*	100 V

the weighting factors are introduced to the cost function. It can be expressed as:

$$
\begin{aligned}
J =&\lambda_1 (i_L(k) - \frac{1-d}{L}\sqrt{i_L(k)V_g\frac{V_o(k)}{i_o(k)}}T_s + \frac{1}{L}V_gT_s - i_L^*)^2 \\
&+ \lambda_2 (V_o(k) + \frac{1-d}{C}i_L(k)T_s - \frac{i_o(k)}{C}T_s - V_o^*)^2
\end{aligned} \tag{12}
$$

where λ_1 denotes the weighting factor for the inductor current objective and λ_2 denotes the weighting factor for the output voltage objective. The selection of the weighting factor will be discussed in the following part.

To make a comparison between the proposed NPI-MPC and only the inductor current control (ICC) based MPC in (6) and (11), Fig. 5 shows the output voltage and uses the parameters in Table I. As seen, although the MPC algorithm with the cost function in (6), which only controls the inductor current can weaken the influence of the NMP behavior, it still cannot guarantee the control accuracy of the output voltage within one prediction horizon. When adopting the proposed control algorithm, it shows a good tracking ability for the output voltage. Another comparison will be discussed between the algorithm used in [22] which utilizes a PI controller to generate the current reference i_L^*. With the introduction of the PI controller, it compensates for the NMP behavior, the output voltage can track the reference well. However, it will reduce the dynamic response speed. The comparison between this PI generated current reference method and the proposed one will be provided in the experiments part.

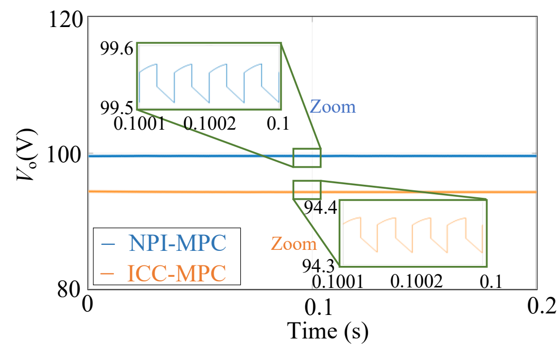

Fig. 5. Output voltage of the NPI-MPC method and the inductor current control based MPC (ICC-MPC) method.

IV. STABILITY ANALYSIS

To guarantee the stable operation of the proposed NPI-MPC, a stability analysis is necessary. However, due to the strong non-linear characteristics which the optimization process performs, the modeling of the NPI-MPC is challenging. In this part, the model of the NPI-MPC controlled boost converter is established through the process of deriving the optimal control variable. After building the entire model, the weighting factors are designed according to its model-based stability.

A. Modeling of the proposed NPI-MPC

The modeling process of the controller is to find the relation between its input and output. In the proposed NPI-MPC, the optimal control variable can be obtained by calculating the derivative of the cost function with respect to duty cycle d which then equals zero and is expressed as:

$$
\frac{\partial[\lambda_1(i_L(k+1) - i_L^*)^2 + \lambda_2(V_o(k+1) - V_o^*)^2]}{\partial d} = 0 \tag{13}
$$

Combining (10) with (13), d can be derived as:

$$
\begin{aligned}
d =& \frac{(i_L(k) - m_1 + \frac{1}{L}V_gT_s - i_L^*)m_1}{-m_1^2 - m_2^2} \\
&- \frac{(V_o(k)(1 - \frac{i_o(k)}{V_o(k)C}T_s + m_2 - V_o^*))m_2}{-m_1^2 - m_2^2}
\end{aligned} \tag{14}
$$

where $m_1 = \sqrt{i_L(k)V_gV_o(k)/i_o(k)}T_s/L$, $m_2 = i_L(k)T_s/C$. To clarify whether the cost function J equals its minimum

TABLE II
THE CALCULATION PROCESS OF THE NPI-MPC.

Algorithm: NPI-MPC algorithm for the boost converter
function: NPI-MPC
1. Measure $i_L(k)$, $V_o(k)$, $i_o(k)$, V_o^*
2. Compute i_L^* with eq. (9)
3. Compute eq. (14)
4. **Return** d_{opt}
5. **if** $0 < d_{opt} < 1$ **then**
6. $d(k) = d_{opt}$
7. **else if** $d_{opt} \leq 0$ **then**
8. $d(k) = 0$
9. **else**
10. $d(k) = 1$
11. **end if**
end function

value when adopting the optimal variable *d*, the second derivative is utilized as follows:

$$\frac{\partial^2 J}{\partial d^2} = 2\frac{d}{L^2} i_L(k) V_g \frac{i_o(k)}{V_o(k)} T_s^2 + 2\frac{d}{C^2} i_L(k)^2 T_s^2 > 0 \quad (15)$$

where *d* lies within (0, 1). According to (15), the second-order derivative of the cost function with respect to control variable *d* is positive. Hence, the cost function will achieve its minimum value when adopting the derived optimal variable *d*.

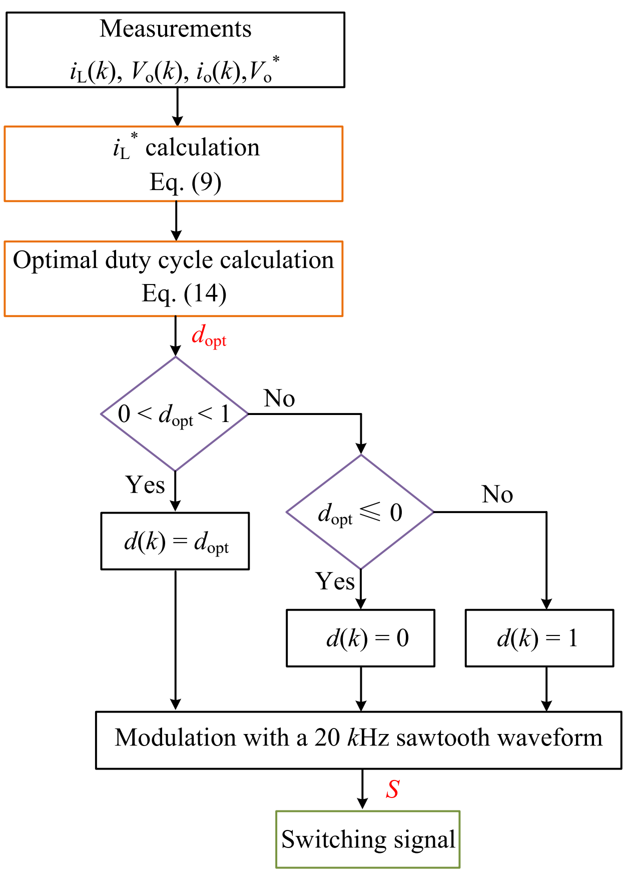

Fig. 6. The flowchart of the proposed NPI-MPC.

B. Stability analysis with different weighting factors

The flowchart of the proposed NPI-MPC is provided in Fig. 6 and the calculation process is presented in Table II. Based on this, the closed-loop transfer function can be obtained by introducing a small signal disturbance. However, the strong nonlinear calculation process in (14) makes it difficult to derive the transfer function without solving high order equations. Therefore, the Jacobian matrix is employed in this paper for the stability analysis method which avoids solving complicated nonlinear equations. The essence of the Jacobian matrix is to fit as close as possible to the desired function near the stable operating point. For the studied system, the function near the stable state point can be expressed as:

$$\begin{aligned} \begin{bmatrix} i_L(k+1) \\ V_o(k+1) \end{bmatrix} &= \begin{bmatrix} F[i_L(k), V_o(k)] \\ G[i_L(k), V_o(k)] \end{bmatrix} \\ &\approx \begin{bmatrix} F(I_L, V_o) \\ G(I_L, V_o) \end{bmatrix} + J_m \begin{bmatrix} F(i_L(k), V_o(k)) \\ G(i_L(k), V_o(k)) \end{bmatrix} \end{aligned} \quad (16)$$

where F and G are the difference equations of the inductor current and output voltage in eq. (10). J_m is the Jacobian matrix. According to the expression of the differential equations in (10), the expression of the Jacobian matrix is expressed as follows:

$$J_m = \begin{bmatrix} J_{m11} & J_{m12} \\ J_{m21} & J_{m22} \end{bmatrix} = \begin{bmatrix} \frac{\partial i_L(k+1)}{\partial i_L(k)} & \frac{\partial i_L(k+1)}{\partial V_o(k)} \\ \frac{\partial V_o(k+1)}{\partial i_L(k)} & \frac{\partial V_o(k+1)}{\partial V_o(k)} \end{bmatrix} \quad (17)$$

J_{m11} - J_{m22} are derived as:

$$\begin{cases} J_{m11} = 1 - \frac{(1-d)T_s\sqrt{V_g \frac{V_o(k)}{i_o(k)}}}{2L\sqrt{i_L(k)}} + \frac{\partial d}{\partial i_L(k)} \sqrt{i_L(k) V_g \frac{V_o(k)}{i_o(k)}} T_s \\ J_{m12} = \frac{\partial d}{\partial V_o(k)} \sqrt{i_L(k) V_g \frac{V_o(k)}{i_o(k)}} T_s \\ J_{m13} = \frac{1}{C} T_s - \frac{i_L}{C} T_s \frac{\partial d}{\partial i_L(k)} - \frac{d}{C} T_s \\ J_{m14} = 1 - \frac{i_L(k)}{C} \frac{\partial d}{\partial V_o(k)} T_s - \frac{i_o(k)}{V_o(k) C} T_s \end{cases} \quad (18)$$

Noticing that the derivative of the inductor current $i_L(k)$ and the output voltage $V_o(k)$ at the kth instant with respect to the optimal control variable d can be derived from (14) as:

$$\begin{cases} \frac{\partial d}{\partial i_L(k)} = \frac{1}{g^2} \left(\frac{\partial f}{\partial i_L(k)} g - \frac{\partial g}{\partial i_L(k)} f \right) \\ \frac{\partial d}{\partial V_o(k)} = \frac{1}{g^2} \left(\frac{\partial f}{\partial V_o(k)} g - \frac{\partial g}{\partial V_o(k)} f \right) \end{cases} \quad (19)$$

where *f* and *g* are the numerator and denominator of *d* in (14) respectively, and the derivatives in (19) are expressed in (20).

$$\begin{cases} \frac{\partial f}{\partial i_L(k)} = \lambda_1 \left(\frac{3}{2} m_1 - m_1^2 + \left(\frac{m_1^2}{2} - \frac{i_L^* T_s}{2L} \right) \sqrt{\frac{V_g \frac{V_o(k)}{i_o(k)}}{i_L(k)}} \right. \\ \left. -\lambda_2 \left(\frac{1}{C} V_o(k) T_s + m_2^2 - \frac{i_o(k)}{V_o(k) C^2} V_o(k) T_s^2 - \frac{V_o^*}{C} T_s \right) \right. \\ \frac{\partial f}{\partial V_o(k)} = -\lambda_2 \left(m_2 - \frac{i_o(k)}{V_o(k) C^2 i_L(k)} T_s^2 \right) \\ \frac{\partial g}{\partial i_L(k)} = -\lambda_2 \frac{2}{C^2} i_L(k) T_s^2 - \lambda_1 m_1^2 \\ \frac{\partial g}{\partial V_o(k)} = 0 \end{cases} \quad (20)$$

Replacing the sampling values $i_L(k)$ and $V_o(k)$ with stable state values I_L and V_o, four parameters J_{m11} - J_{m12} can be obtained. The stability criterion is satisfied when the eigenvalues are in the unit circle. Otherwise, it is unstable. Fig. 7(a) provides the eigenvalue e_1 derived from the Jacobian matrix in (17). To simplify the calculation, we determine that λ_2 equals the unit value. When the ratio of the weighting factors λ_1 and λ_2 changes from 0 to 10 (λ_1 changes from 0 to 10), the amplitudes of the eigenvalue e_1 are always lower than the unit value, so it will not influence the system's stability. Taking eigenvalue e_2 into consideration in Fig. 7(b), it is evident that the amplitude of the eigenvalue will exceed the unit value with the λ_1 ratio smaller than 0.25.

The trend can be described as: with the growth of the weighting factor ratio λ_1 to λ_2, the amplitude of the eigenvalue $e_2$decreases, while the amplitude of the eigenvalue e_2 increases when the ratio decreases. This phenomenon can be explained according to equations (7), (8), and (12). The weighting factor λ_1 determines the weight for the control of the inductor current control in the cost function where it will not lead to instability when operating. However, the weighting factor λ_2 denotes the weight for the output voltage control in the cost function. It will lead to instability when operating because of the unstable behavior existing in the control of the output transfer function in (7). Hence, when it increases, the system tends to be unstable.

Fig. 8 shows the output voltage based NPI-MPC with different weighting factors in the stable state and unstable state, respectively. It can be seen when the λ_1 is larger than 0.25 and equals 6.67, the system can track the output voltage reference stably and accurately. However, when the λ_1 is smaller than 0.25 which equals 0.15, the output cannot track the reference well.

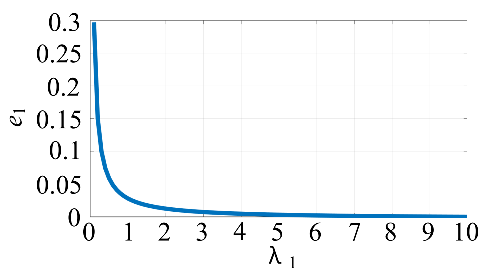

(a) Amplitude of eigenvalue e_1.

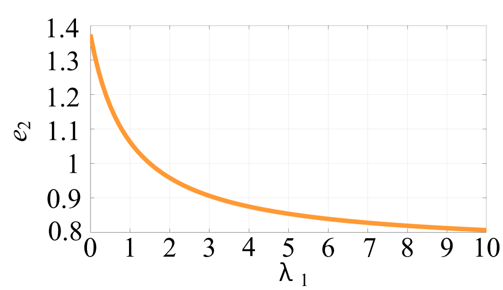

(b) Amplitude of eigenvalue e_2.

Fig. 7. The amplitudes of eigenvalues and stability boundary with different weighting factors.

C. Inductance and Capacitor Design

In the design process, the selection of passive components is important which closely influences the system's performance. In this part, the stability of the various inductances and capacitors with different weighting factors are assessed to compare the stable boundary. As seen in Fig. 9(a), the colored region presents the stable region, and the blank part presents

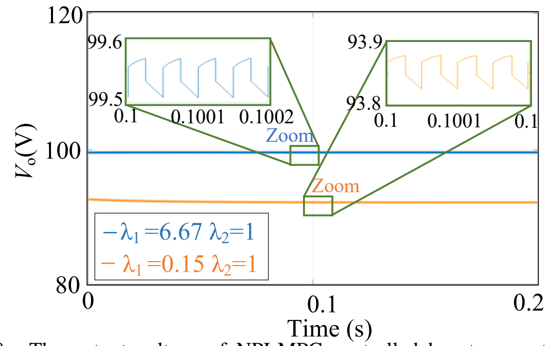

Fig. 8. The output voltage of NPI-MPC controlled boost converter using different weighting factors.

the unstable region with various inductances. When λ_1 is larger than 0.4, it shows that the system will be stable if the inductance changes from 500 μH to 1.5 mH. When λ_1 is smaller than 0.4, with the increase of the inductances the stability region is decreased. Similarly, in Fig. 9 (b), the

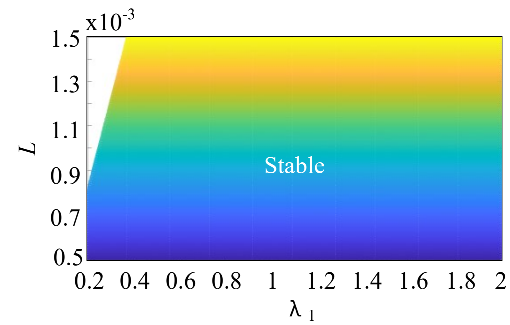

(a) Stability regions (colored part) with different inductances.

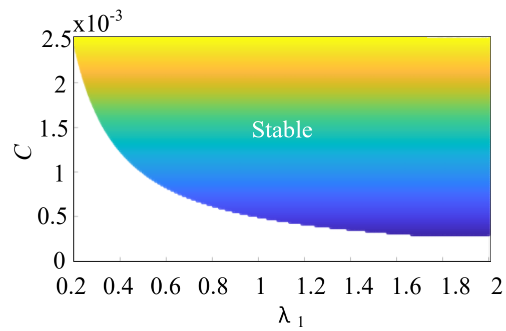

(b) Stability regions (colored part) with different capacitors.

Fig. 9. Stable region with different inductances and capacitors with NPI-MPC.

colored region presents the stable region, and the blank part shows the unstable region with various capacitors. When λ_1 changes from 0.2 to 2, it shows that the stable region will increase if the capacitor increases from 500 μF to 2.5 mF. Fig. 10 shows the output voltage with the same weighting factors, λ_1 = 0.3 and λ_2 = 1, and different inductance L = 500 μH and L = 1.5 mH which are from stable and unstable regions in Fig. 10 (a) respectively. It shows that the output voltage is well tracked when using the inductance L = 500 μH. Fig. 10 (b) shows the output voltage with the same weighting factors, λ_1 = 0.6 and λ_2 = 1, and different capacitors C = 1 mF and C = 500 μF which are from stable and unstable regions in Fig. 10(b) respectively. It shows that the output voltage reference is well tracked when using the capacitor C = 1 mF.

This article has been accepted for publication in IEEE Transactions on Industrial Electronics. This is the author's version which has not been fully edited and content may change prior to final publication. Citation information: DOI 10.1109/TIE.2023.3247785

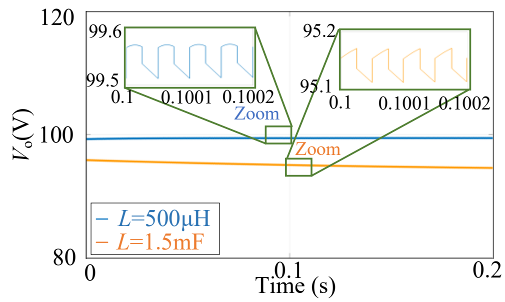

(a) Output voltage with inductance L = 500 μH and L = 1.5 mH with λ_1 = 0.3, λ_2 = 1.

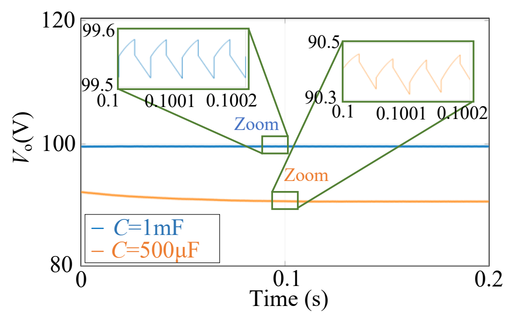

(b) Output voltage with capacitor C = 1 mF and C = 500 μF with λ_1 = 0.6, λ_2 = 1.

Fig. 10. Simulations of output voltage using different weighting factors and systems' parameters.

V. EXPERIMENTS

To verify the proposed NPI-MPC algorithm and the above analysis, a boost converter with 50 V input and 100 V output was built in the lab. The DC source is supported by a Delta Elektronika SM 600-10 dc power supply. The dSPACE DS1202 board is used to implement the NPI-MPC algorithm. Besides, a PWM Generation is used to generate a 20-kHz symmetrical sawtooth for generating the desired PWM. Fig. 11 shows the experimental prototype. Table I shows the system's parameters and the control parameters.

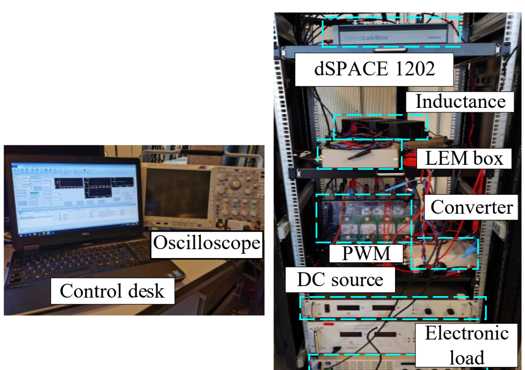

Fig. 11. Experimental set up.

A. Case Study 1: Comparison between proposed NPI-MPC and conventional MPC algorithm

This case makes a comparison between the proposed NPI-MPC algorithm and the conventional MPC based on (5) of the boost converter. According to the results in Fig. 12 (a), when adopting the conventional MPC, the output voltage cannot track its reference. When replacing with the proposed NPI-MPC in Fig. 12 (b), the output voltage tracks the reference.

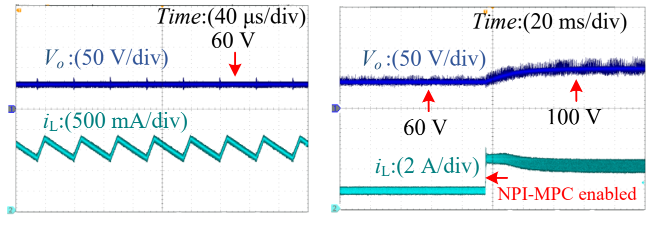

(a) Conventional MPC. (b) Change from the conventional MPC to the NPI-MPC.

Fig. 12. Behavior of the conventional MPC and the proposed NPI-MPC.

As seen, the NPI-MPC can prevent the tracking failure of the output voltage caused by the NMP behavior.

B. Case Study 2: The NPI-MPC controlled Boost converter with input and output step

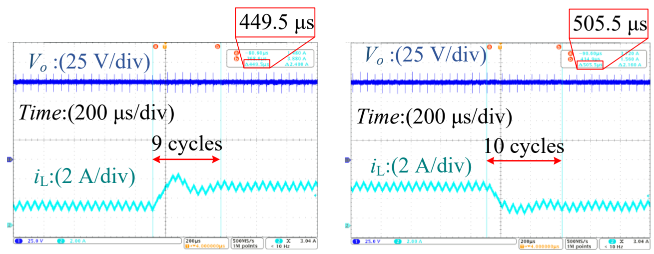

(a) Load steps from 100 W to 200 W. (b) Load steps from 200 W to 100 W.

Fig. 13. Output voltage V_o and inductor current i_L with the proposed NPI-MPC during load steps.

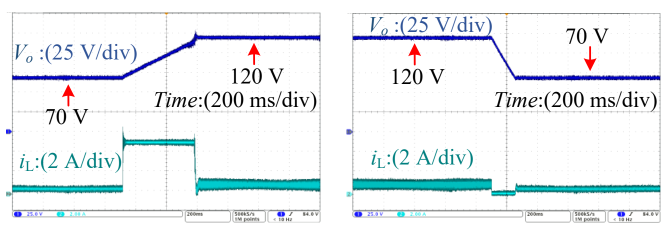

(a) Output reference steps from 70 V to 120 V. (b) Output reference steps from 120 V to 70 V.

Fig. 14. Output voltage V_o and inductor current i_L with the proposed NPI-MPC during voltage reference steps.

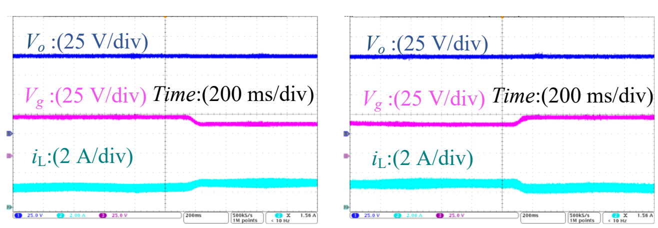

(a) Input voltage steps from 50 V to 40 V. (b) Input voltage steps from 40 V to 50 V.

Fig. 15. Output voltage V_o and inductor current i_L with the proposed NPI-MPC during input voltage steps.

The second case provides a load step, output voltage reference step, and input voltage change with the NPI-MPC and weighting factors λ_1 = 2, λ_2 = 1. The output power of the load steps from 100 W to 200 W and 200 W to 100 W in Fig. 13. According to the results, when the output power changes, it only takes a few switching cycles, which is approximately 450 μs and 500 μs to adjust the inductor current into the

This article has been accepted for publication in IEEE Transactions on Industrial Electronics. This is the author's version which has not been fully edited and content may change prior to final publication. Citation information: DOI 10.1109/TIE.2023.3247785

stable state without obvious overshoot concerns. Besides, the average frequency can be evaluated as 1/(449.5 μs/9) = 20 kHz, 1/(505.5 μs/10) = 19.8 kHz and they are approximately equal to the desired 20 kHz. Fig. 14 presents the dynamic process when the output voltage reference changes from 70 V to 120 V and 120 V to 70 V with the same weighting factors. As seen, with the NPI-MPC, the system can track the output voltage reference accurately. Fig.15 studies the behavior of output voltage when input voltage steps from 50 V to 40 V and 40 V to 50 V. As observed, the output voltage can maintain its reference value without any overshoot concerns, which shows a good adjusting ability.

C. Case Study 3: Comparison study

Given to the methods in [20] and [21] employ a complicated design process, it is not necessary to compare because the proposed one is easier to implement. Hence, this case compares the method in [22] which used the PI to generate a current reference and established a tunable switching frequency. The parameter of the PI module is selected as $K_p = 0.1$, $K_i = 10$. The comparison study will be carried out with frequency changes and dynamic process.

Fig.16 shows a tunable frequency change with the proposed method. The frequency can transit smoothly from 20 kHz to 12.5 kHz or 12.5 kHz to 20 kHz respectively. It proves the proposed NPI-MPC can easily change the switching frequency to a desired value.

Fig. 17 shows the dynamic process with the proposed algorithm when the load changes. Comparably, Fig. 18 shows the dynamic process of PI generated current reference based MPC algorithm with the same load change. It is obvious the proposed algorithm performs a better adjusting ability with fast response speed which is approximately 500 μs as well as less overshoot. However, the PI combined MPC algorithm takes approximately 300 ms to reach the new stable state during the dynamic process and has an overshoot of 20 V.

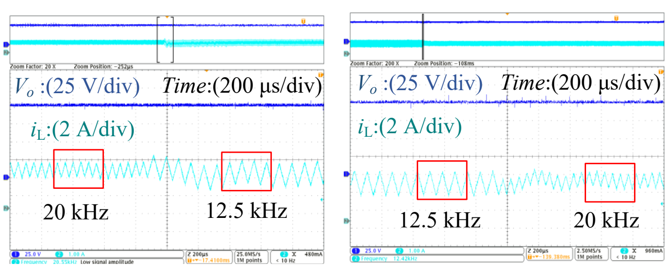

(a) Switching frequency changes from 20 kHz to 12.5 kHz. (b) Switching frequency changes from 12.5 kHz to 20 kHz.

Fig. 16. Output voltage V_o and inductor current i_L with the proposed NPI-MPC during switching frequency changes.

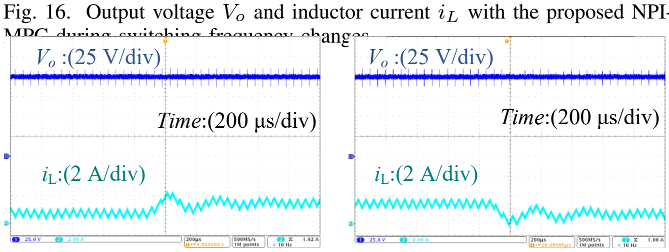

(a) Load steps from 50 W to 100 W. (b) Load steps from 100 W to 50 W.

Fig. 17. Output voltage V_o and inductor current i_L with the proposed NPI-MPC during load steps.

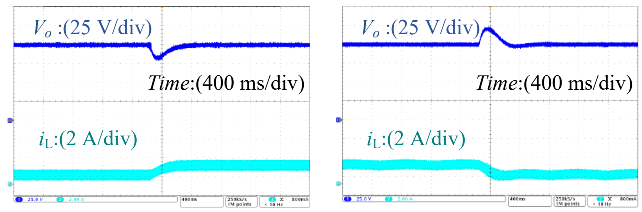

(a) Load steps from 50 W to 100 W. (b) Load steps from 100 W to 50 W.

Fig. 18. Output voltage V_o and inductor current i_L with the PI combined MPC during load steps.

D. Case Study 4: Stability validation of the NPI-MPC algorithm with different weighting factors

This case investigates the effects of different weighting factors on the NPI-MPC algorithm. According to the above analysis presented in Fig. 19, four groups of weighting factors are tested. As seen from the results, when adopting the first group of weighting factors $\lambda_1 = 0.25$, $\lambda_2 = 1$ in the unstable region, the system occurs the loss of regulation in output voltage. When adopting the second group of weighting factors $\lambda_1 = 2$, $\lambda_2 = 1$ in the stable region, the system can track the output voltage well and the switching frequency remains constant. Next, when adopting the third and fourth groups of weighting factors $\lambda_1 = 0.2$, $\lambda_2 = 1$ in the unstable region, and $\lambda_1 = 3$, $\lambda_2 = 1$ in the stable region. It can be seen that the tracking failure occurs when adopting $\lambda_1 = 0.2$, and $\lambda_2 = 1$. Hence, the control performance relies heavily on the weighting factors in the cost function. And the stable region gives a guideline for selecting the weighting factors for the cost function to ensure the tracking ability.

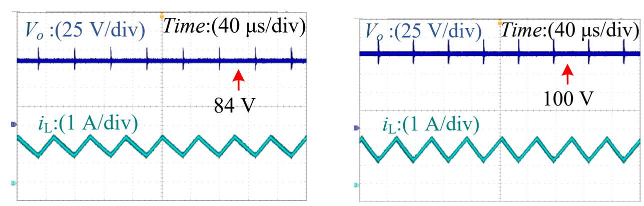

(a) $\lambda_1 = 0.25$, $\lambda_2 = 1$ (b) $\lambda_1 = 2$, $\lambda_2 = 1$

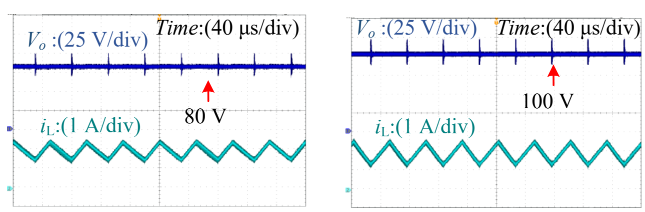

(c) $\lambda_1 = 0.2$, $\lambda_2 = 1$ (d) $\lambda_1 = 3$, $\lambda_2 = 1$

Fig. 19. Output voltage V_o and inductor current i_L with the NPI-MPC using different weighting factors.

E. Case Study 5: The proposed NPI-MPC with the mismatch of parameters

In a real application, the inductance may vary due to the current level and the capacitor will degrade with the age. Therefore, it is necessary to test the robustness of the proposed method when the parameters mismatch between the real values and that used in the MPC. This case presents the robustness of the proposed method with the mismatch of the parameters. The value of the parameters is changed by the control desk. In order to provide the waveforms of output voltage and inductance

TABLE III
COMPARISON OF DIFFERENT CONTROL METHODS WITH PROPOSED NPI-MPC.

Description	[20]	[21]	[22]	NPI-MPC
Complexity	Complicated due to the use of input linearization	Complicated due to the use of observer and the design of the dynamic inductor current value	Simple	Simple
Switching frequency f_s	Control of f_s is not studied But it is time-varying	Fixed	Approximately fixed But varying during the dynamic process	Fixed
Dynamic response	Short	Short	Moderate	Short
Parameters design requirements	Input linearization Weighting factor design is not studied but is needed	Observer and N^* which is related to the dynamic inductor current value need to be designed	PI controller, possible weighting factor design with more control objectives	Weighitng factor
Robustness	Not robust Additional error compensated action is needed	Not robust	Not robust But the effect of parameter mismatch is acceptable	Robust

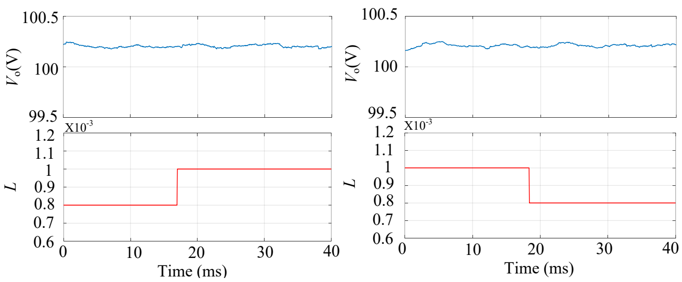

(a) Inductance value changes from 0.8 mH to 1 mH (b) Inductance value changes from 1 mH to 0.8 mH.

Fig. 20. Output voltage V_o with the mismatch of L with the proposed NPI-MPC.

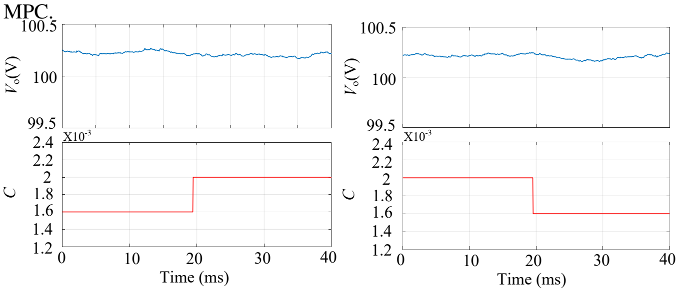

(a) Capacitor value changes from 1600 μF to 2000 μF (b) Capacitor value changes from 2000 μF to 1600 μF.

Fig. 21. Output voltage V_o with the mismatch of C with the proposed NPI-MPC.

value/capacitor value used in the MPC synchronously. Hereby, we capture the waveforms measuring from the control desk of dSPACE. In both cases, the weighting factors are λ_1 = 1, λ_2 = 1. Fig. 20 shows the output voltage with the change of inductance value used in the model from 0.8 mH to 1 mH and 1 mH to 0.8 mH. It is evident that the output voltage is maintained at its reference value during the step process. Also, when the capacitor value used in the model changes from 2000 μF to 1600 μF and 1600 μF to 2000 μF in Fig. 21, the output voltage tracks its reference value 100V well. Hence, the proposed method shows good robustness when parameters mismatch.

Finally, to summarize the comparison of the proposed methods and other typical methods, Table III is presented to illustrate in detail.

VI. CONCLUSION

This paper proposes an NPI-MPC algorithm for the boost converter. Firstly, the actual cause behind the NMP behavior in conventional MPC controlled boost converter is analyzed. And then a modified inductor difference equation is proposed. Besides, to generate a fixed switching frequency, the optimal value of the duty cycle is derived and then modulated.

It is proved that for the boost converter, the proposed NPI-MPC improves the NPM behavior. The output voltage can track its reference only with a single prediction horizon which avoids long computation time. And the switching frequency remains fixed equaling the frequency of the sawtooth. Moreover, the model of the proposed NPI-MPC is established. And the Jacobian matrix is carried out for the stability assessment with different parameters. From the stability analysis results, it can be concluded that when designing weighting factors, the larger ratio between λ_1 and λ_2 is prone to be stable. When designing inductances and capacitors for the system, the smaller inductance and larger capacitors are prone to be stable with the proposed NPI-MPC controlled boost converter. In the end, the experimental results prove the effectiveness of the proposed NPI-MPC algorithm which ensures stable operation, fast dynamic response as well as robustness.

REFERENCES

[1] J. M. Guerrero, J. C. Vasquez, J. Matas, et.al, " Hierarchical control of droop-controlled ac and dc microgrids—a general approach toward standardization," *IEEE Trans Ind. Electron.*, vol. 58, no. 1, pp. 158-172, Jan. 2011.

[2] S. Anand and B. G. Fernandes, " Reduced-order model and stability analysis of low-voltage DC microgrid," *IEEE Trans Ind. Electron.*, vol. 60, no. 11, pp. 5040-5049, Nov. 2013.

[3] T. Dragičević, X. Lu, J. C. Vasquez, et.al, "DC microgrids—Part I: A review of control strategies and stabilization techniques," *IEEE Trans Power Electron.*, vol. 31, no. 7, pp. 4876-4891, Jul. 2016.

[4] S. Sahoo, T. Dragičević and F. Blaabjerg, "An event-driven resilient control strategy for DC microgrids", *IEEE Trans Power Electron.*, vol. 35, no. 12, pp. 13714-13724, Dec. 2020.

[5] Z. Karami, Q. Shafiee, S. Sahoo, et al, "Hybrid model predictive control of DC-DC boost converters with constant power load," *IEEE Trans. Energy Convers.*, vol. 36, no. 2, pp. 1347-1356, Jun. 2021.

[6] T. Dragičević, S. Vazquez and P. Wheeler, "Advanced control methods for power converters in DG systems and microgrids," *IEEE Trans Ind. Electron.*, vol. 68, no. 7, pp. 5847-5862, Jul. 2021.

[7] V. Paduvalli, R. J. Taylor, and P. T. Balsara, "Analysis of zeros in a boost DC-DC converter: state diagram approach," *IEEE Trans. Circuits Syst., II, Exp. Briefs*, vol. 64, no. 5, pp. 550–554, May 2017.

[8] S. K. Pandey, S. L. Patil, and S. B. Phadke, "Regulation of nonminimum phase DC-DC converters using integral sliding mode control combined with a disturbance observer," *IEEE Trans. Circuits Syst., II, Exp. Briefs*, vol. 65, no. 11, pp. 1649–1653, Nov. 2018.

This article has been accepted for publication in IEEE Transactions on Industrial Electronics. This is the author's version which has not been fully edited and content may change prior to final publication. Citation information: DOI 10.1109/TIE.2023.3247785

[9] R. J. Wai and L. C. Shih, “Design of voltage tacking control for DC-DC boost converter via total sliding-mode technique,” *IEEE Trans Ind. Electron*., vol. 58, no. 6, pp. 2502–2511, Jun. 2011.

[10] M. Leng, G. Zhou, Q. Tian, et.al, ”Small signal modeling and design analysis for boost converter with valley V2 control,” *IEEE Trans Power Electron*., vol. 35, no. 12, pp. 13475-13487, Dec. 2020.

[11] S. Kouro, P. Cortes, R. Vargas, et.al, “Model predictive control: A simple and powerful method to control power converters,” *IEEE Trans. Ind*., vol. 56, no. 6, pp. 1826-1838, Jun. 2009.

[12] S. Vazquez, J. Rodriguez, M. Rivera, et.al, ”Model predictive control for power converters and drives: Advances and trends,” *IEEE Trans. Ind*., vol. 64, no. 2, pp. 935-947, Feb. 2017.

[13] T. Dragičević, “Dynamic stabilization of DC microgrids with predictive control of point of load converters,” *IEEE Trans Power Electron*., vol. 33, no. 12, pp. 10872–10884, Dec. 2018.

[14] O. Andrés-Martínez, A. Flores-Tlacuahuac, O. F. Ruiz-Martinez et.al, ”Nonlinear model predictive stabilization of DC–DC boost converters with constant power loads,” *Journ. Emerg. Sel. Topics Power Electron*., vol. 9, no. 1, pp. 822-830, Feb. 2021.

[15] P. Karamanakos, T. Geyer, and S. Manias, ”Direct voltage control of DC-DC boost converters using enumeration-based model predictive control,” *IEEE Trans Power Electron*., vol. 29, no. 2, pp. 968–978, Feb. 2014.

[16] A. Ayad, P. Karamanakos and R. Kennel, ”Direct model predictive current control strategy of quasi-Z-source inverters,” *IEEE Trans Power Electron*., vol. 32, no. 7, pp. 5786-5801, Jul. 2017.

[17] P. Karamanakos, T. Geyer, and R. P. Aguilera, “Long-horizon direct model predictive control: modified sphere decoding for transient operation,” *IEEE Trans. Ind. Appl*., vol. 54, no. 6, pp. 6060–6070, Nov.-Dec. 2018.

[18] T. Dorfling, H. du Toit Mouton, T. Geyer, et.al, ”Long-horizon finite-control-set model predictive control with nonrecursive sphere decoding on an FPGA, ”*IEEE Trans Power Electron*., vol. 35, no. 7, pp. 7520–7531, Jul. 2020.

[19] E. Zafra, S. Vazquez, C. Regalo, et al., ”Parallel sphere decoding algorithm for long-prediction-horizon FCS-MPC,” *IEEE Trans Power Electron*., vol. 37, no. 7, pp. 7896-7906, Jul. 2022.

[20] F. A. Villarroel, J. R. Espinoza, M. A. Pérez, et al., ”Stable shortest horizon FCS-MPC output voltage control in non-minimum phase boost-type converters Based on Input-State Linearization,” *IEEE Trans. Energy Convers*., vol. 36, no. 2, pp. 1378-1391, Jun. 2021.

[21] L. Cheng, P. Acuna, R. P. Aguilera, et al., ”Model predictive control for DC-DC boost converters with reduced-prediction horizon and constant switching frequency,” *IEEE Trans Power Electron*., vol. 33, no. 10, pp. 9064-9075, Oct. 2018.

[22] N. Guler, S. Biricik, S. Bayhan, and H. Komurcugil, “Model predictive control of DC-DC SEPIC converters with auto-tuning weighting factor,” *IEEE Trans. Ind*., vol. 68, no. 10, pp. 9433–9443, Oct. 2021.

[23] M. Novak, U. M. Nyman, T. Dragicevic, et.al., ”Analytical design and performance validation of finite set MPC regulated power converters,” *IEEE Trans. Ind*., vol. 66, no. 3, pp. 2004-2014, Mar. 2019.

[24] P. Cortes, G. Ortiz, J. I. Yuz, et.al, “Model predictive control of an inverter with output LC filter for UPS applications,” *IEEE Trans. Ind*., vol. 56, no. 6, pp. 1875–1883, Jun. 2009.

[25] F. Villarroel, J. R. Espinoza, C. A. Rojas, et.al, “Multiobjective switching state selector for finite-states model predictive control based on fuzzy decision making in a matrix converter,” *IEEE Trans. Ind*., vol. 60, no. 2, pp. 589–599, Feb. 2013.

[26] J. Rodriguez and P. Cortes, Predictive control of power converters and electrical drives. Hoboken, NJ, USA: Wiley, 2012.

[27] T. Dragičević and M. Novak, ”Weighting factor design in model predictive control of power electronic converters: An artificial neural network approach,” *IEEE Trans. Ind*., vol. 66, no. 11, pp. 8870-8880, Nov. 2019.

[28] C. Panjapornpon and M. Soroush, ”Shortest-prediction-horizon non-linear model-predictive control with guaranteed asymptotic stability,” *Int. J. Control*, vol. 80, no. 10, pp. 1533–1543, Sep. 2007.

Yuan Li (S’20) received the B.Sc. & M.Sc. degree in Electrical Engineering from Southwest Jiaotong University, Chengdu, China in 2017 & 2020, respectively. She is currently working toward the Ph.D. degree with AAU Energy, Aalborg University, Aalborg, Denmark.

Her research interests include modeling of power converters, stability analysis of dc microgrid, and model predictive control for power converters.

Subham Sahoo (S’16-M’18) received the B.Tech. & Ph.D. degree in Electrical and Electronics Engineering from VSSUT, Burla, India and Electrical Engineering at Indian Institute of Technology, Delhi, New Delhi, India in 2014 & 2018, respectively. He is currently an Assistant Professor and a vice-leader for Reliability of Power Electronic Converters (ReliaPEC) research group in the Department of Energy, AAU, Denmark. He is a recipient of the Indian National Academy of Engineering (INAE) Innovative Students Project Award for the best PhD thesis across all the institutes in India for the year 2019. He was also a distinguished reviewer for IEEE Transactions on Smart Grid in the year 2020.

His research interests are control, optimization, cybersecurity and stability of power electronic dominated grids, physics-informed machine learning tools for power electronic systems.

Tomislav Dragičević (S’09–M’13–SM’17) received the M.Sc. and the industrial Ph.D. degrees in electrical engineering from the Faculty of Electrical Engineering, University of Zagreb, Zagreb, Croatia, in 2009 and 2013, respectively. From 2013 until 2016, he has been a Postdoctoral Researcher with Aalborg University, Aalborg, Denmark. From 2016 until 2020, he was an Associate Professor with Aalborg University, Denmark. He is currently a Professor with the Technical University of Denmark, Kongens Lyngby, Denmark. He made a Guest Professor stay with Nottingham University, Nottingham, U.K., during spring/summer of 2018. He has authored and coauthored more than 330 technical publications (more than 150 of them are published in international journals, mostly in IEEE), 10 book chapters and a book in this field, as well as filed for several patents. His research interests include application of advanced control, optimization and artificial intelligence inspired techniques to provide innovative and effective solutions to emerging challenges in design, control, and diagnostics of power electronics intensive electrical distributions systems and microgrids.

He serves as an Associate Editor for the IEEE TRANSACTIONS ON INDUSTRIAL ELECTRONICS, IEEE TRANSACTIONS ON POWER ELECTRONICS, IEEE EMERGING AND SELECTED TOPICS IN POWER ELECTRONICS, and IEEE INDUSTRIAL ELECTRONICS MAGAZINE.

Yichao Zhang (S’20) received the B.Sc. & M.Sc. degree in Electrical Engineering from Southwest Jiaotong University, Chengdu, China in 2017 & 2020, respectively. She is currently working toward the Ph.D. degree with AAU Energy, Aalborg University, Aalborg, Denmark.

Her research interests include energy storage system plan and control, frequency stability analysis, and machine learning.

Frede Blaabjerg (S’86–M’88–SM’97–F’03) was with ABB-Scandia, Randers, Denmark, from 1987 to 1988. From 1988 to 1992, he got a Ph.D. degree in Electrical Engineering at Aalborg University in 1995. He became an Assistant Professor in 1992, an Associate Professor in 1996, and a Full Professor of power electronics and drives in 1998. From 2017 he became a Villum Investigator. He is honoris causa at University Politehnica Timisoara (UPT), Romania, and Tallinn Technical University (TTU) in Estonia. His current research interests include power electronics and its applications, such as in wind turbines, PV systems, reliability, harmonics, and adjustable speed drives.

He has received 32 IEEE Prize Paper Awards, the IEEE PELS Distinguished Service Award in 2009, the EPE-PEMC Council Award in 2010, the IEEE William E. Newell Power Electronics Award 2014, the Villum Kann Rasmussen Research Award 2014, the Global Energy uPrize in 2019 and the 2020 IEEE Edison Medal. He was the Editor-in-Chief of the IEEE Transactions on Power Electronics from 2006 to 2012. He has been a Distinguished Lecturer for the IEEE Power Electronics Society from 2005 to 2007 and for the IEEE Industry Applications Society from 2010 to 2011 as well as 2017 to 2018. In 2019-2020 he served a President of the IEEE Power Electronics Society. He is Vice-President of the Danish Academy of Technical Sciences too. He is nominated in 2014-2019 by Thomson Reuters to be between the most 250 cited researchers in Engineering in the world.